Neurobiology:

Targeting the Transient Receptor Potential Vanilloid Type 1 (TRPV1) Assembly Domain Attenuates Inflammation-induced Hypersensitivity

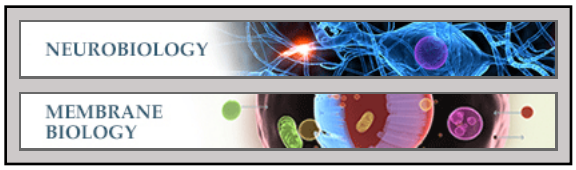

Robyn Flynn, Kevin Chapman, Mircea Iftinca, Reem Aboushousha, Diego Varela and Christophe Altier

J. Biol. Chem. 2014, 289:16675-16687.
doi: 10.1074/jbc.M114.558668 originally published online May 7, 2014

THE JOURNAL OF BIOLOGICAL CHEMISTRY VOL. 289, NO. 24, pp. 16675–16687, June 13, 2014

Targeting the Transient Receptor Potential Vanilloid Type 1 (TRPV1) Assembly Domain Attenuates Inflammation-induced Hypersensitivity*

Received for publication, February 19, 2014, and in revised form, April 25, 2014 Published, JBC Papers in Press, May 7, 2014, DOI 10.1074/jbc.M114.558668

Robyn Flynn[‡], **Kevin Chapman**[‡], **Mircea Iftinca**[‡], **Reem Aboushousha**[‡], **Diego Varela**[§1], **and Christophe Altier**[‡2]

From the [‡]*Department of Physiology and Pharmacology and Snyder Institute for Chronic Diseases, University of Calgary, Calgary, Alberta T2N 4N1, Canada and* [§]*Centro de Estudios Moleculares de la Celula and Instituto de Ciencias Biomedicas, Facultad de Medicina, Universidad de Chile, Santiago, 8380453, Chile*

Background: Assembly of TRPV1 subunits forms functional channels that transduce noxious stimuli.
Results: We identified a region of the TRPV1 C terminus that mediates subunit assembly and used a disrupting peptide to block association.
Conclusion: A short C-terminal motif enables subunit association. Disrupting assembly of TRPV1 subunits attenuates inflammatory hyperalgesia.
Significance: TRPV1 subunit association could be targeted for pain relief.

The transient receptor potential channel vanilloid type 1 (TRPV1) is a non-selective cation channel expressed in sensory neurons of the dorsal root and trigeminal ganglia. TRPV1 is a polymodal channel activated by noxious heat, capsaicin, and protons. As a sensor for noxious stimuli, TRPV1 channel has been described as a key contributor to pain signaling. To form a functional channel, TRPV1 subunits must assemble into tetramers, and several studies have identified the TRPV1 C terminus as an essential element in subunit association. Here we combined biochemical assays with electrophysiology and imaging-based bimolecular fluorescence complementation (BiFC) and bioluminescence resonance energy transfer (BRET) in live cells to identify a short motif in the C-terminal tail of the TRPV1 subunit that governs channel assembly. Removing this region through early truncation or targeted deletion results in loss of subunit association and channel function. Importantly, we found that interfering with TRPV1 subunit association using a plasma membrane-tethered peptide attenuated mechanical and thermal hypersensitivity in two mouse models of inflammatory hyperalgesia. This represents a novel mechanism to disrupt TRPV1 subunit assembly and hence may offer a new analgesic tool for pain relief.

The TRPV1[3] channel, also called the capsaicin receptor, is found in small- to medium-diameter primary sensory ganglia neurons (trigeminal and nodose ganglia) that respond to physical and chemical noxious stimuli (nociceptors). An important feature of the TRPV1 channel is its polymodal mechanism of activation. TRPV1 is a sensor for capsaicin (1), noxious heat (>43 °C), low pH, toxins (2–4), and arachidonic acid metabolites (5). Acute stimulation of TRPV1 leads to a burning sensation, reflecting a central role of this channel in nociception. Pharmacological and genetic studies have confirmed its contribution/modulation in several models of pathological pain (6). For instance, TRPV1 null mice show virtually no thermal hyperalgesia during inflammation (7). Furthermore, rapid desensitization of TRPV1-expressing fibers by administration of the potent agonist resiniferatoxin attenuates experimental inflammatory hyperalgesia and neurogenic inflammation as well as naturally occurring cancer pain and debilitating arthritic pain (8).

Structurally, TRPV1 channels are composed of four subunits surrounding a central pore; each subunit contains six transmembrane domains flanked by long intracellular N- and C-terminal extensions. To function as nociceptors, TRPV1 subunits must assemble into tetramers (9) as well as be exported to the cell membrane. Previous biochemical and functional investigations of the molecular determinants of TRPV1 assembly have identified the C-terminal tail of the channel as the assembling domain (10, 11), yet the exact motif of interaction remains controversial. Although one study found the TRP domain, an ~24-residue helix just downstream of the sixth transmembrane region, to promote TRPV1 subunit association (10), another group identified a more distal motif comprising residues 752–772 (termed the tetrameric assembly domain (TAD)) (11). The recent release of a high resolution single-particle electron cryomicroscopy (cryo-EM) structure of an assembled TRPV1 channel has highlighted the interactions of a β sheet from one subunit, composed of a C-terminal β strand and two β strands from the N terminus, with the N-terminal ankyrin repeat domain of an adjacent subunit (9). Unfortunately, the specific residues of the C-terminal strand involved in subunit associa-

* This work was supported by the Heart and Stroke Foundation of Canada and the Canadian Institute of Health Research.
[1] Recipient of Fondo Nacional de Ciencia y Tecnologia Grant 1120240.
[2] This author holds a Canada Research Chair in Inflammatory Pain (Tier2). To whom correspondence should be addressed: Dept. of Physiology and Pharmacology and Snyder Institute for Chronic Diseases, University of Calgary, 3330 Hospital Dr. N.W., Calgary, Alberta T2N 4N1, Canada. Tel.: 403-220-7549; E-mail: altier@ucalgary.ca.
[3] The abbreviations used are: TRPV1, transient receptor potential channel vanilloid type 1; TAD, tetrameric assembly domain; BRET, bioluminescence resonance energy transfer; BiFC, bimolecular fluorescence complementation; MIA, monoiodoacetate; ANOVA, analysis of variance; VN, VenusN; VC, VenusC; AKAP, A kinase anchoring protein.

tion could not be assigned, and the structure did not extend to the region of the C terminus purported to contain a subunit assembly domain.

Our study aimed to identify the region of the C terminus that is responsible for TRPV1 assembly and trafficking. In addition to using western blotting analysis, calcium imaging, electrophysiology, and confocal microscopy, we took advantage of BRET methodology and fluorescence complementation conjugated with BRET to visualize and quantify TRPV1 subunit oligomerization in live cells. This study identifies a previously unrecognized region of 17 residues, flanked by the TRP domain and the TAD, to be involved in TRPV1 subunit association. Finally, we found that a palmitoyl-conjugated peptide mimicking this motif that disrupted subunit interaction (12) could reduce hyperalgesia in two distinct murine models of inflammatory pain.

EXPERIMENTAL PROCEDURES

Plasmids—The rat TRPV1-pcDNA5/FRT expression vector was a generous gift from Dr. A. Patapoutian and was used as a PCR template to create fusion proteins. TRPV1-YFP was made by introducing EcoRI and KpnI sites and cloned into pEYFP-N1. The hemi-Venus BiFC system consists of a 240-residue Venus molecule, an improved variant of YFP, that has been divided into VenusN (158 residues) and VenusC (82 residues). Close proximity of the two moieties allows them to reform a Venus molecule and emit a fluorescence signal. TRPV1 and TRPV4 BiFC constructs were made by subcloning the channel into the BspEI/XbaI sites of VenusN-Zipper and VenusC-Zipper (13). These VenusN-TRPV1, VenusC-TRPV1, VenusN-TRPV4, and VenusC-TRPV4 constructs were created by cloning the channel 3′ to the hemi-Venus moiety with a 10-amino acid linker (GGGGSGGGGS) in between (13, 14). CD4-TRPV1 C-terminal and N-terminal constructs were generated by PCR using primers containing NotI/XbaI restriction sites. C-terminal truncations of Venus-TRPV1 were made by introducing premature stop codons into the TRPV1 sequence by site-directed mutagenesis at residues Leu-773, Trp-752, Gly-734, and Cys-715. TRPV1-Luciferase was made by cloning the TRPV1 coding sequence into pRLuc-N3. We created GFP-tagged short fragments of the TRPV1 C terminus by cloning annealed sticky-ended oligonucleotides comprising the sequences of TRPV1 residues 716–733, 734–751, or 752–772 into a custom HA-myc vector then into pEGFP-C3. TRPV1 containing an extracellular HA epitope (TRPV1-HA) was made by introducing a ClaI restriction site between residues His-614 and Lys-615, located in the S5-S6 linker upstream of the p loop, then cloning in sticky-ended annealed oligonucleotides coding for the HA sequence. TRPV1-YFP deletion mutants were made by loop-out mutagenesis using partially overlapping primers (15) to delete residues 716–733, 734–751, or 752–772. The CD4-AA cell surface marker was a generous gift from Dr. Zamponi and is described in Altier *et al.* (16). The CD4-Nt2 was made by subcloning the coding sequence corresponding to residues 155–308 of rat TRPV1into CD4-AA; the CD4-Ct was made by subcloning the full-length C terminus (682–838) into CD4-AA using NotI and XbaI sites. The hTRPM8 was a kind gift from Dr. Rithwik Ramachandran.

Cell Culture and Transfection—Human embryonic kidney tsA-201 cells were cultured as described previously (16). Cells were transfected at ~50% confluence using the calcium phosphate method. For imaging, cells were plated on MatTek dishes coated overnight with polyornithine (0.002%).

Immunocytochemistry and Confocal Microscopy—To visualize HA-tagged TRPV1 and CD4-tagged constructs, cells were fixed in 4% paraformaldehyde 48 h post transfection, permeabilized with 0.05% Triton-X100, and immunostained with anti-HA (1/1000, Roche Applied Science) or anti-CD4 (1/1000, eBioscience). Alexa-594-conjugated anti-rat and Alexa-594-conjugated anti-mouse were used as secondary antibody for HA and CD4, respectively. Confocal images were collected on a Zeiss LSM-510 Meta inverted microscope using either a 40× water immersion or a 63× oil 1.4NA oil immersion lens. Venus/YFP was visualized by excitation with an argon laser (514 nm), and emission was detected using a long-pass 530-nm filter. Enhanced GFP was visualized by excitation at 488 nm. Alexa-594 antibody was visualized by excitation with a HeNe laser (543 nm), and emission was detected using a 585–615-nm band-pass filter. Image acquisition was performed with identical gain, contrast, laser excitation, pinhole aperture, and laser scanning speed.

BRET and BiFC-BRET—tsA-201 cells were co-transfected with TRPV1-RLuc and either TRPV1-YFP (for BRET) or VN- and VC-TRPV1 mutants (for BiFC-BRET). Cells were washed with PBS, detached in PBS + 10 mM EDTA, resuspended in PBS, and then divided into a black 96-well plate (Greiner Bio-one) to measure the total YFP fluorescence or a white 96-well plate (Brand) for BRET assay. Total YFP fluorescence was counted in a Victor 2 plate reader (PerkinElmer Life Sciences) using an excitation filter of 485 nm and emission filter of 530 nm. BRET signal was measured in a Mithras LB940 (Berthold Technologies) after incubating the cells with the RLuc substrate coelenterazine-h (5 μM) for 5 min. BRET measurement was calculated as the ratio of YFP emission (530 nm) to RLuc emission (460 nm). BRET signal was expressed as net BRET, which is the signal from YFP/RLuc less the signal from RLuc alone.

Co-immunoprecipitation and Western Blotting—Cells were harvested 48 h after transfection and lysed in radioimmunoprecipitation assay buffer (0.1% SDS, 1% Triton X-100, and 0.5% sodium deoxycholate in PBS) with Complete EDTA-free protease inhibitor (Roche Applied Science) for 1 h on ice. Cell lysates were precipitated with a mix of protein A and protein G beads incubated with antibody with overnight rotation at 4 °C. Beads and precipitates were washed 3× in radioimmunoprecipitation assay buffer then eluted from beads in 1× Laemmli buffer. Samples were run on 8% Tris-glycine gels and transferred to nitrocellulose membranes, then probed with rabbit anti-GFP (Torrey Pines) 1:5000 followed by ECL-optimized anti-rabbit (GE Healthcare). For peptide interference assays, cells co-expressing HA-TRPV1 and TRPV1-YFP were harvested and pelleted, then resuspended in 600 μl of cold PBS. 200 μM TRPV1 peptide, 200 μM scrambled peptide or an equal volume of DMSO was added to the 100 μl of cells, and they were rotated at 4 °C for 1 h. Cells were again pelleted and lysed in radioimmunoprecipitation assay buffer with protease inhibitor.

Proteins were precipitated with rat HA antibody (Roche Applied Science) coupled to protein G beads.

Peptides and Behavioral Experiments—N-terminally palmitoylated peptides were obtained from Genemed Synthesis (San Antonio, TX) with at least 90% purity with the following sequences: TRPV1, 734–752, KDDYRWCFRVDEVNWTTW; scrambled, TTWVDEWNFCRWDYRDKV. Male c57bl/6 mice aged 6 weeks were obtained from Charles River Canada and housed with free access to food and water with a 12/12 light dark cycle. All experiments were conducted on aged-matched animals under protocols approved by the University of Calgary Animal Care Committee and in accordance with the international guidelines for the ethical use of animals in research and guidelines of the Canadian Council on Animal Care.

To induce osteoarthritis, mice received a single intra-articular injection (10 μl) of sodium monoiodoacetate (MIA, 2.5 mg/ml, Sigma) in the right knee or the saline vehicle in the contralateral knee under isofluorane anesthesia. Osteoarthritis was allowed to develop for 15 days. Before nociception testing, mice were habituated to the behavior room for 1 h. For peptide injection and testing, a base-line mechanical withdrawal threshold was determined in both hind paws with von Frey hairs using the modified up-down method of Dixon (17, 18). Mice were injected with 10 μl of TRPV1 peptide (from a 10 μM stock in 75% DMSO, 25% saline) into the footpad or by intrathecal route between L5 and L6. Nociceptive responses were tallied as positive if the animal exhibited paw withdrawal, licking and/or biting, during or immediately after stimulation. Data are presented as a 50% mechanical threshold for each group ± S.E.

For the carrageenan test, the right hind paw was injected with 10 μl of 2% λ-carrageenan (in saline, Sigma) along with 10 μM TRPV1 or scrambled peptide. Mice were tested for paw withdrawal latency using the Hargreaves apparatus from Ugo Basile (Comerio, Italy). Briefly, mice on glass plates were subjected to targeted infrared heat under the injected paw, and the paw withdrawal latency was determined by motion-sensing software. Each time point was done in triplicate.

Calcium Imaging—Cells transiently expressing TRPV1 and TRPM8 were loaded with Fluo-4 (1 μM for 30 min, Invitrogen) along with 10 μM TRPV1 or scrambled peptide in extracellular solution containing 135 mM NaCl, 5 mM KCl, 3 mM $CaCl_2$, 2 mM $MgCl_2$, 10 mM D-glucose, 10 mM HEPES; pH was adjusted to 7.3. We perfused capsaicin (200 nM, Sigma) at a rate of ~2 ml/min to examine TRPV1 activity, then followed with menthol (30 μM, sigma) to activate TRPM8. To assess calcium signals, cells were imaged using a 20× objective on an Olympus IX51 microscope controlled by cellSens software. Images were acquired every 500 ms and processed using ImageJ by drawing discrete regions of interest around cells that responded to menthol. We expressed a change in fluorescence as a -fold change from base line normalized to background fluorescence ($\Delta F/F_0$).

Electrophysiology—Whole-cell patch clamp experiments on HEK cells were performed 16–24 h after transfection with calcium phosphate (16). The internal pipette solution contained 140 mM CsCl, 5 mM NaCl, 1 mM $MgCl_2$, 1 mM BAPTA, 0.45 mM $CaCl_2$ and was adjusted to pH 7.2 with CsOH. The bath solution contained 100 mM NaCl, 2 mM $CaCl_2$, 1 mM $MgCl_2$, 10 mM glucose, 95 mM sorbitol, and 10 mM HEPES; pH 7.4 was adjusted with NaOH. Patch clamp experiments were performed using an Axopatch 200B amplifier, and pClamp 9.2 software was used for data acquisition and analysis (both from Molecular Devices Corp., Sunnyvale, CA). Data were digitized at 10 kHz and low pass-filtered at 1 kHz. Patch electrodes (~3 megaohm resistance) were pulled from borosilicate glass (Warner Instruments, Hamden CT) using a BB-CH puller (Mecanex SA, Geneva, Switzerland). When applicable, voltages were corrected for liquid junction potentials. All experiments were conducted at 22 ± 2 °C.

Statistical Analysis—Statistical analysis was conducted via *t* tests or one way analysis of variance (ANOVA) followed by Dunnett's multiple comparison tests. Statistical significance was set at $p < 0.05$, and all *error bars* represent S.E.

RESULTS

Detection of TRPV1 Homomers by BiFC and BiFC/BRET Assay—To visualize recombinant TRPV1 subunit oligomerization in live cells, we used BiFC, in which two proteins of interest are fused to hemi-Venus moieties. If the distance between TRPV1 subunits is compatible with complementation of the Venus moieties, subunit association will yield YFP fluorescence. We fused the TRPV1 subunit to either the N-terminal (VN) or the C-terminal (VC) fragment of the Venus moiety (Fig. 1*A*). When co-expressed in HEK cells, recombinant VN-TRPV1 and VC-TRPV1 showed YFP fluorescence, indicating that TRPV1 subunits assemble into dimers and/or higher order multimers (Fig. 1*B*, *upper left panel*). Notably, the YFP fluorescence was not observed upon expression of VN-TRPV1 or VC-TRPV1 alone (data not shown). Next, we co-transfected the hemi-Venus constructs with a HA-TRPV1 to verify that fusion to the Venus fragments did not disrupt TRPV1 trafficking. Imaging of cells expressing both Venus and Alexa-visualized HA tag revealed a clear fluorescence overlap of channel subunits at both intracellular location and the plasma membrane, as illustrated with the line scan in Fig. 1*B*.

To complement the BiFC results with a medium throughput BRET assay, we created a TRPV1 fused to Renilla luciferase (Rluc) as an energy donor and used the combined (VN-TRPV1 and VC-TRPV1) as the acceptor. The resulting BiFC-BRET signal reflects the assembly of trimeric, tetrameric, and perhaps higher order multimeric forms of the channels. After expression of the recombinant TRPV1 subunits, the net BRET value (BRET signal − background BRET from TRPV1-Rluc alone) was plotted as a function of VN-TRPV1+VC-TRPV1 concentration. The specificity of the BiFC-BRET signal was characterized by the saturation curve illustrated in Fig. 1*C*. Importantly, specific BiFC-BRET signal was lost when replacing the VC-TRPV1 with the VC-TRPV4 construct. Altogether, these data demonstrate the formation of homomeric TRPV1 receptors and validate the TRPV1 BiFC and BRET constructs as a valuable tool set to monitor channel assembly in live cells.

The TRPV1 Subunit Interaction Domain Lies in the C Terminus—To pinpoint a specific multimerization motif using the BiFC and BiFC-BRET approaches, we generated a series of Venus-TRPV1 mutants by introducing premature stop codons in the C-terminal tail at residues 773 (downstream of the TAD),

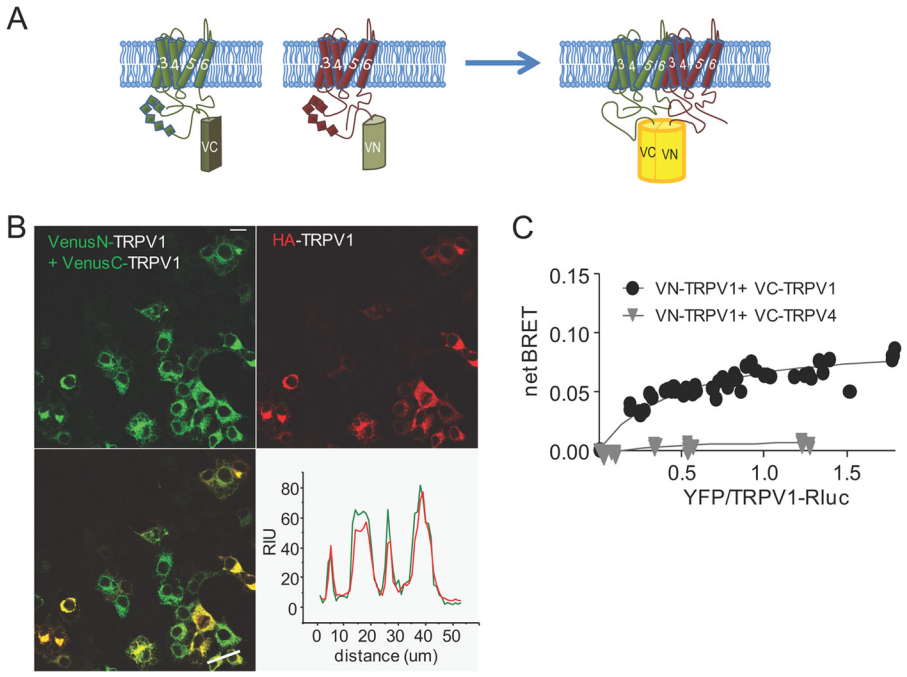

FIGURE 1. **Measure of TRPV1 subunits interaction by BiFC and BRET-BiFC.** *A*, schematic representation of the hemi-Venus proteins (N and C moieties) fused to the N terminus of TRPV1. A functional Venus molecule is formed by protein complementation, resulting from TRPV1 subunit association. *B*, representative image of tsA-201 cells co-transfected with VenusN-TRPV1 + VenusC-TRPV1 and HA-TRPV1. Note the YFP signal that results from VenusN-TRPV1 and VenusC-TRPV1 association and fluorescence complementation. *Lower right*, line scan analysis of VenusN-TRPV1 + VenusC-TRPV1 (*green*) co-transfected with HA-TRPV1 (*red*) shows overlap of fluorescent signal. *Scale bar* = 10 μm. RIU = relative intensity units. *C*, BRET-BiFC titration curve from tsA-201 cells co-transfected with increasing amounts of [VenusN-TRPV1 + VenusC-TRPV1] or [VenusN-TRPV1 + VenusC-TRPV4] and a constant amount of TRPV1-RLuc as the energy donor. Saturation of the BRET-BiFC curve indicates specific TRPV1 interaction, whereas the low linear BRET-BiFC signal denoted the absence of TRPV1 interaction with the TRPV4 channel. Data from three experiments are included in the graph.

752 (upstream of the TAD), 734 (downstream of the proximal PIP2 binding region), and 715 (downstream of the coiled coil motif) (Fig. 2*A*). Before using these constructs in a BiFC assay, we confirmed the expression of each VenusC mutant by western blotting analysis. To determine subunit association, we co-expressed the single mutant with VN-TRPV1 WT and visualized fluorescence complementation by confocal microscopy (Fig. 2*B*). Total fluorescence intensity was reduced to background level with the Gly-734 and Cys-715 and somewhat reduced in the Trp-752, indicating a pronounced loss of interaction of these mutants with a full-length TRPV1 subunit (Fig. 2*B histogram*).

This apparent requirement of residues 715–752 for subunit interaction was also tested by co-immunoprecipitation experiments using HA-tagged full-length TRPV1 to precipitate VN-TRPV1 mutants. The HA-TRPV1 showed interaction with VN-TRPV1 full-length and Leu-773 and Trp-752 mutants but not with the Gly-734 and Cys-715 mutants (Fig. 2*C*). Strikingly, although we used VN-fused TRPV1 mutants for BiFC imaging but VC-fused mutants for precipitation, both methods provided similar results, confirming a key role of the 715–752 region for TRPV1 subunit assembly.

Given that functional TRPV1 channels are tetramers, we examined whether residues 715–752 can govern the assembly of higher order multimers (>dimers). We took advantage of the fact that three or more subunits must come together to produce BiFC-BRET signal and tested our VC-TRPV1 truncation mutants with VN-TRPV1 full-length and TRPV1-Rluc in this assay. Net BiFC-BRET signal was markedly reduced when the VC-TRPV1 subunit was truncated at residues 715 or 734, indicating an absence of channel multimers (Fig. 2*D*). Similar BRET results were obtained when co-expressing VN-TRPV1 mutants with VC-TRPV1 (data not shown), suggesting that the particular Venus moiety fused to TRPV1 mutants did not affect its interactions. These data thus establish that the minimal motif for TRPV1 subunit assembly is encompassed by residues 715 and 752.

Identification of Residues 734–751 for TRPV1 C Termini Interaction—We sought to examine whether the assembly of TRPV1 subunits occurs through direct interaction of their C termini, as suggested previously (19), as well as to narrow down a minimal interaction motif. We created expression vectors of GFP-tagged peptides comprised of residues 716–733, 734–751, and 752–772, a region that was recently reported to be the TAD (11). We expressed these GFP peptides alone or with a TRPV1 C terminus fused to the CD4 membrane receptor (CD4-Ct) and examined the subcellular localization of the GFP signal to determine direct interaction between GFP peptides and the membrane-tethered CD4-Ct. Expressed alone, GFP peptides were diffusely distributed through the cytosol (Fig. 3*A*, *left panel*). When co-expressed with CD4-Ct, both of the two distal motifs (734–751 and 752–772) were found to be translocated to the plasma membrane, indicating an interaction with the membrane-tethered CD4-Ct, whereas the subcellular localization of the proximal 716–733 region remained cytosolic (Fig. 3*A*, *center* and *right panels*). This effect is illustrated in line scans of cells in Fig. 3*A*, *right panel* (Fig. 3*B*) and quantified in Fig. 3*C* using the ratio of GFP fluorescence between the mem-

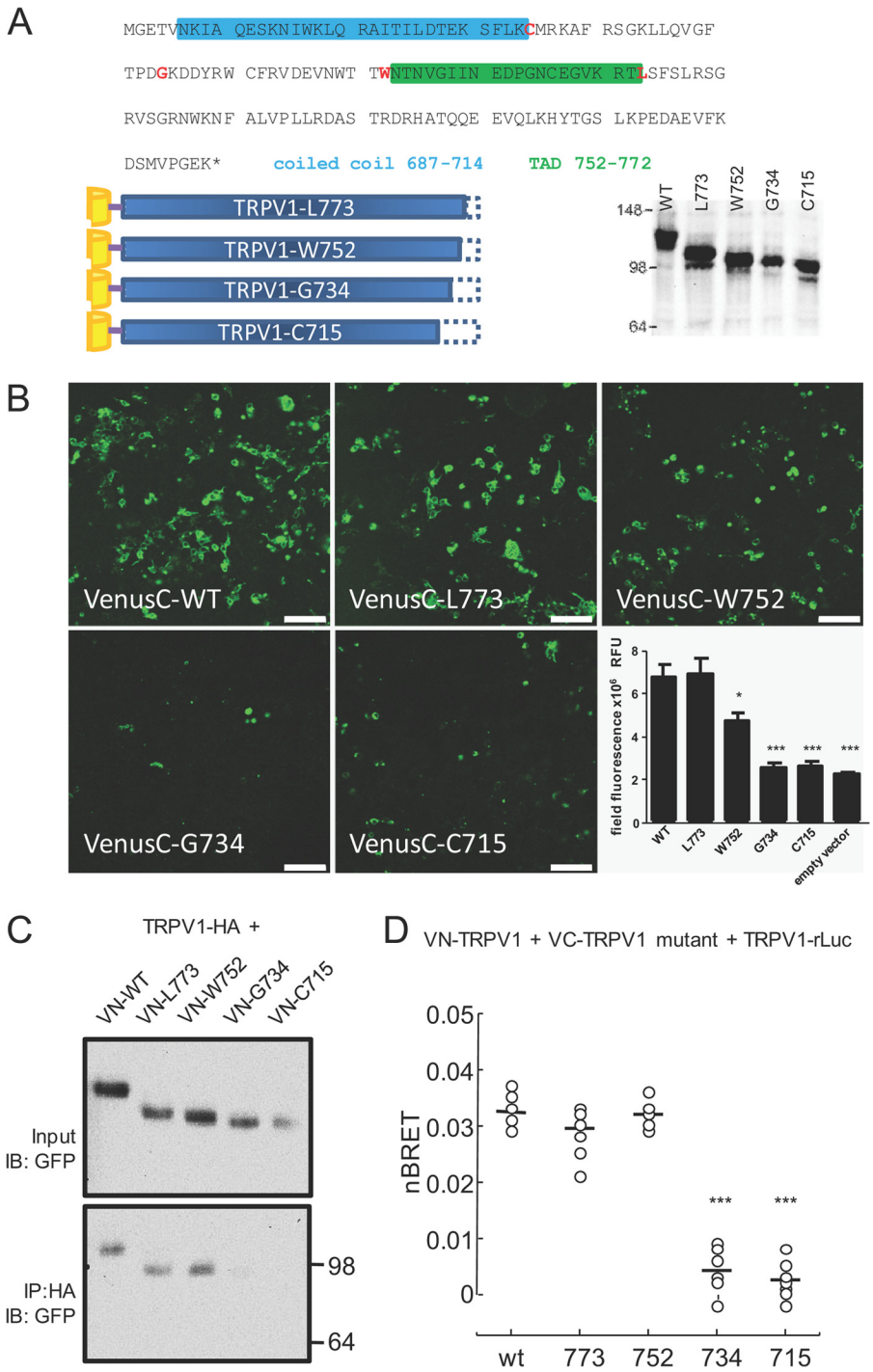

FIGURE 2. **TRPV1 subunit interaction occurs in the C terminus.** *A*, TRPV1 truncation mutations. *Top*, stop codons were introduced at residues (in *red*) Cys-715, Gly-734, Trp-752, and Leu-773; coiled-coil and TADs are identified by colored boxes (*blue*, coiled-coil; *green*, TAD). *Lower left*, truncated mutants were N-terminally tagged with VenusN or VenusC. *Lower right*, mutant expression was verified by western blot analysis from transfected tsA-201 cell lysates (data are representative of three independent experiments). *B*, TRPV1 subunit association relies on the C terminus. Confocal images of truncated TRPV1 mutants N-terminally fused to VenusC (as indicated in *A*) or control empty vector (VenusN-zipper) co-expressed with the full-length VenusN-TRPV1. The fluorescent signal indicates subunit association; *scale bar* = 100 μm. *Lower right*, quantitation of field fluorescence indicated that truncating the TRPV1 subunit shorter than Trp-752 results in loss of subunit association (*, $p < 0.05$; ***, $p < 0.001$, one-way ANOVA, $n = 14–16$ images for each mutant and empty vector). *RFU*, relative fluorescence units. *C*, co-immunoprecipitation of VenusN-tagged truncated mutants with full-length HA-tagged TRPV1 shows loss of subunit interaction with shorter TRPV1 proteins ($n = 3$ independent experiments). *Upper panel*, input membrane immunoblotted (*IB*) with antibody to GFP which recognizes VenusN protein. *Lower panel*, HA-TRPV1 was immunoprecipitated with HA antibody, and TRPV1 mutants were detected with GFP antibody. Molecular masses in kDa are indicated on the *right*. *D*, subunit interaction measured by BRET-BiFC. Venus-tagged truncated mutants were co-expressed with Venus-tagged and luciferase-tagged full-length TRPV1. BRET-BiFC experiments were conducted as in Fig. 1*C* except that a fixed amount (500 ng each) of VenusN+ VenusC acceptor was used for the assay. This amount of acceptor was found to achieve BRET-BiFC saturation in the titration curve of WT TRPV1 (VN-TRPV1 + VC-TRPV1. ***, $p < 0.01$, ANOVA followed by Tukey's multiple comparison test). *n*BRET = net BRET.

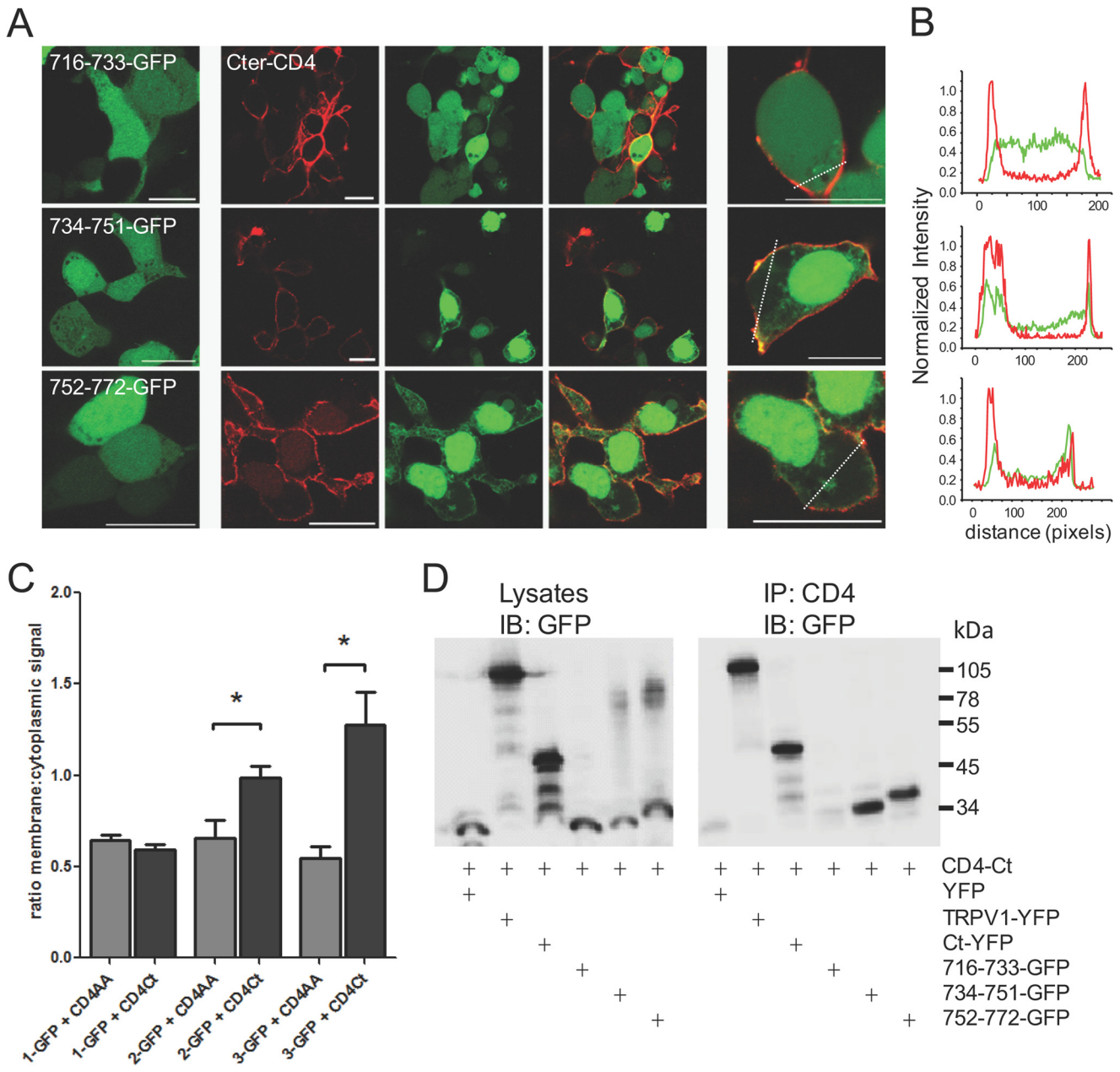

FIGURE 3. **Small TRPV1 C-terminal peptides 734–751 and 752–772 interact with the full-length C terminus.** *A*, the three GFP-tagged fragments of the TRPV1 C terminus were co-expressed in tsA-201 cells with the membrane-tethered CD4-tagged TRPV1 C terminus. Interaction between the peptide and the full-length C terminus results in translocation of the GFP signal to the membrane. *Left panel*, GFP-tagged peptide alone. *Center panels*, GFP-tagged peptide (*green*) co-expressed with CD4-C terminus (*red*). *Right panels*, higher magnification images of center panels; all *scale bars* = 20 μm. *B*, line scans from cells in the *right panel* of *A* indicating that peptides 734–751 and 752–772 are present at the cell membrane with the CD4-C terminus, whereas peptide 716–733 exhibits diffuse distribution within the cell. *C*, *bar chart* representing the ratio (mean ± S.E.) of membrane:cytoplasmic signal of GFP-tagged peptides. The 734–751 and 752–772 show membrane translocation when co-expressed with the membrane-tethered CD4-tagged TRPV1 C terminus (CD4Ct, *black bars*) as compared with CD4-tagged control (CD4AA, *gray bars*). *, $p < 0.05$, ANOVA, followed by Dunnett's multiple comparison test. $n = 6$–21 cells per transfection. *D*, co-immunoprecipitation of GFP-tagged peptides with the full-length CD4-tagged C terminus of TRPV1. 734–751 and 752–772 co-precipitate with CD4-tagged TRPV1 C terminus. *Left panel*, input lysates immunoblotted (*IB*) for GFP; *right panel*, CD4-tagged TRPV1 C terminus immunoprecipitates (*IP*) the TRPV1 channel, the C terminus, and the 734–751 as well as the 752–772 peptides but not the 716–733 peptide. Transfected tsA cell lysates were immunoprecipitated with the anti-CD4 antibody and blotted for GFP. Molecular masses in kDa are indicated on the *right*. Data are representative of three independent experiments.

brane and the cytosolic compartment. As a control, the effect of CD4-AA, the membrane-tethered construct not fused to the TRPV1 C terminus was compared with CD4-Ct (16).

Next, we conducted a co-immunoprecipitation assay with the same constructs to confirm this interaction. Using the CD4 tag to precipitate complexes, we showed that CD4-Ct interacted with the full-length TRPV1 subunit, a YFP-tagged TRPV1 C terminus, and the 734–751 and 752–772 fragments but not the 716–733 region (Fig. 3*D*) containing part of the TRP-like domain (10). Thus, we have identified two contiguous motifs located in the C-terminal region of TRPV1 that promote channel assembly through interactions with the C termini of adjacent TRPV1 subunits.

Deleting C-terminal Regions Identifies Residues 734–751 as Critical for Subunit Association—To test the role of our GFP-tagged C-terminal peptides on both channel function and

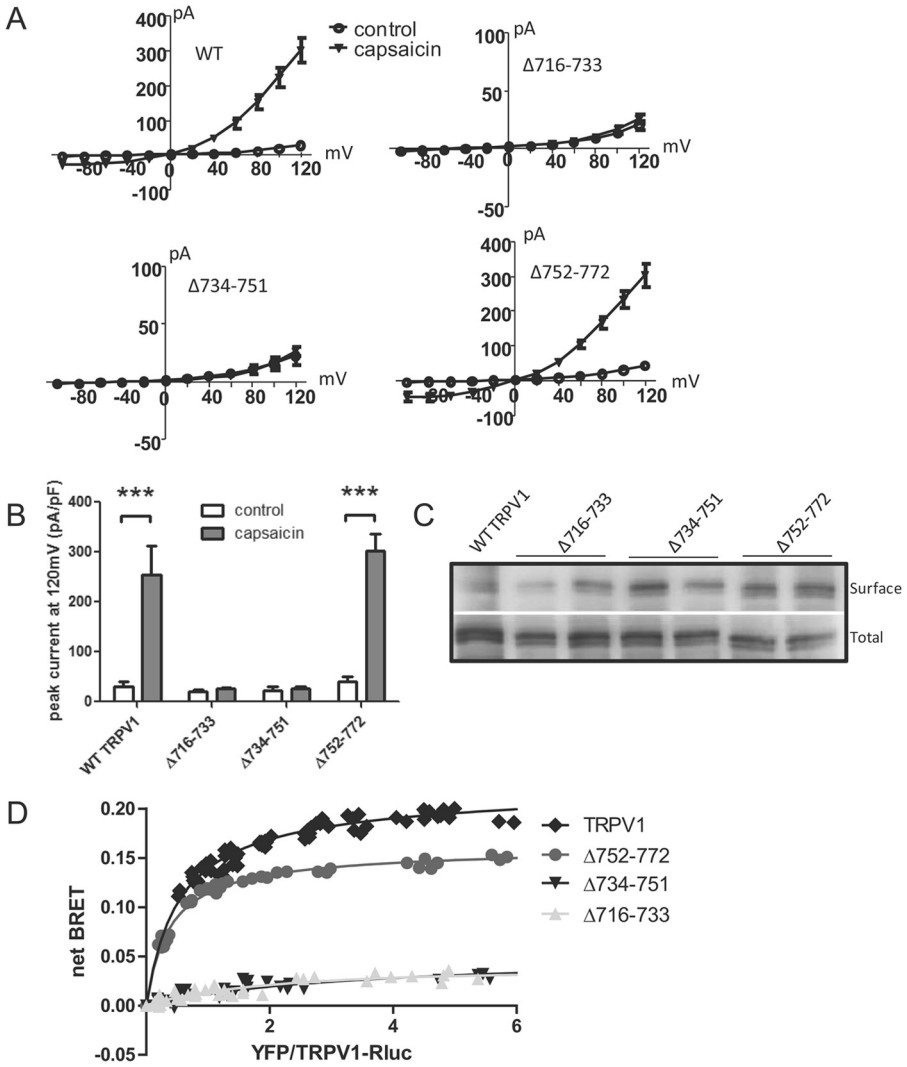

FIGURE 4. **Deleting residues 734–751 abolished subunit association and TRPV1 channel function without affecting surface trafficking.** *A*, whole-cell patch clamp recordings reveal tsA cells expressing full-length TRPV1 or Δ752–772-TRPV1, but not Δ716–733-TRPV1 or Δ734–751-TRPV1, showed robust capsaicin-evoked currents ($n = 3$–7 cells). *B*, *bar chart* representing the peak current density at +120mV before and after application of capsaicin. *Error bars* indicate S.E. *pF*, picofarads. *C*, western blot of surface biotinylated YFP-tagged TRPV1 mutants transfected in tsA-201 cells ($n = 5$ independent experiments). Note that deleting residues of the TRPV1 C terminus does not substantially affect subunit expression at the plasma membrane. *Top*, surface biotinylation of TRPV1-YFP (*one lane*) and deletions (*two lanes each*); *bottom*, total TRPV1 protein expression, both probed with anti-GFP. *D*, BRET titration curve of YFP-tagged TRPV1 mutants co-expressed with WT TRPV1-Rluc channel. Deleting residues 716–733 and 734–751 results in a low linear BRET signal, which indicates the absence of interaction. Saturation of the BRET curve indicates specific TRPV1 interaction with Δ752–772-TRPV1. All deletions were significantly different from WT, $p < 0.001$, by one-way ANOVA. Data from three experiments are included in the graph.

membrane trafficking, we used loop-out mutagenesis to remove each of the three regions examined in Fig. 3 from the full-length YFP-tagged TRPV1 channel, creating Δ716–733, Δ734–751, and Δ752–772. Electrophysiological recordings of these mutants revealed robust capsaicin-evoked current for the WT YFP-TRPV1 and the Δ752–772 TRPV1 mutant, whereas the Δ716–733 and Δ734–751 channels were non-responsive (Fig. 4, *A* and *B*). We next used surface biotinylation to determine whether the non-responsive Δ716–733 TRPV1 and Δ734–751 TRPV1 were retained in the endoplasmic reticulum. Surprisingly, every mutant showed substantial membrane expression similar to that of WT TRPV1 (Fig. 4*C*), revealing that 1) removal of the subunit assembling domain eliminated channel function without affecting cell surface expression and 2) mutant channels unable to form oligomers are still able to be trafficked to the cell surface. To confirm that deleting the two proximal regions did indeed eliminate subunit association, we tested the ability of these YFP-tagged mutants to associate with WT TRPV1-Rluc using BRET. In fact, deleting 752–772 had little effect on subunit association, whereas removing 716–733 or 734–751 seemed to abolish it entirely (Fig. 4*D*), although western blotting analysis indicated similar levels of expression for WT and mutant channels.

Our collective results demonstrate that of the three contiguous C-terminal regions studied, only region 734–751 is both necessary, in that it interacts directly with the C terminus of the TRPV1 subunit (Fig. 3), and essential, in that deleting this regions abolishes subunit association (Fig. 4). Because the 734–751 motif appears to have a dominant role in controlling subunit assembly and thus channel function at the cell surface, we focused our subsequent experiments on this specific region.

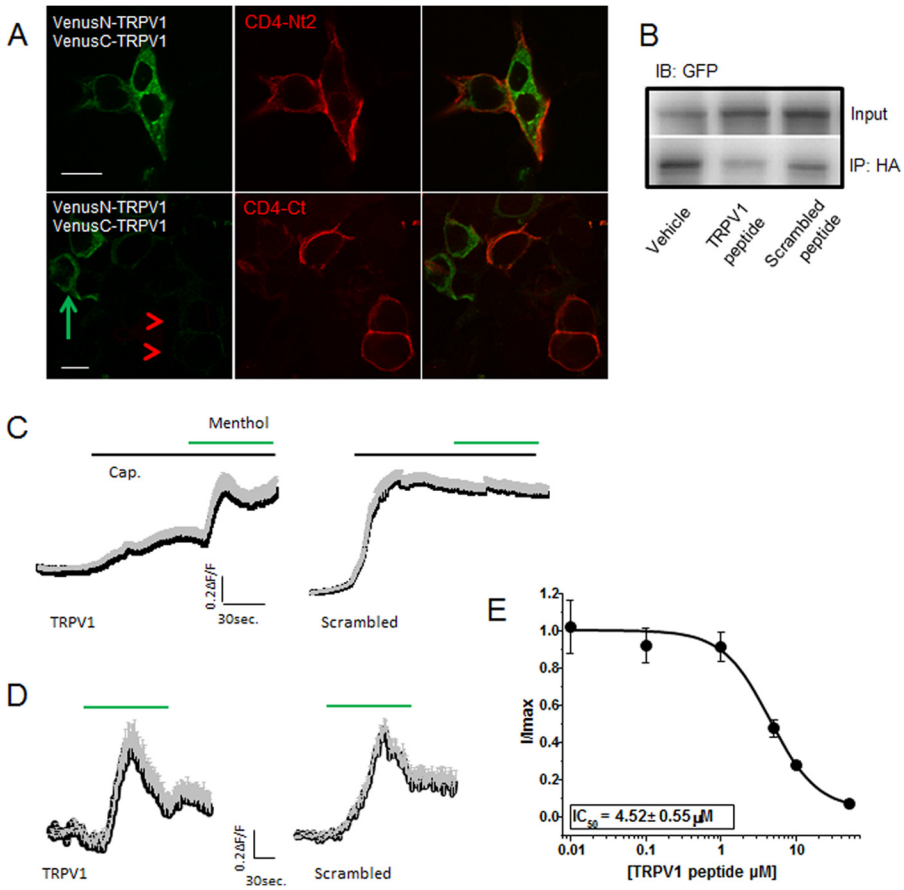

FIGURE 5. **TRPV1 peptides interfere with TRPV1 subunit association.** *A*, expression of the CD4-tagged TRPV1 C terminus interferes with TRPV1 subunit association. tsA-201 cells were transfected with VN-TRPV1, VC-TRPV1, and either the CD4-tagged TRPV1 N-terminal fragment (*CD4-Nt2*) or the CD4-tagged TRPV1 C terminus (*CD4-Ct*). *Top*, cells co-expressing the Venus-TRPV1 proteins (*green* signal upon subunit association) with the N-terminal fragment (*red*) show *green* and *red* signals in the same cell, indicating that the N-terminal fragment does not interfere with subunit association. *Bottom*, cells co-expressing Venus-TRPV1 proteins and the C terminus show no green signal where the red signal is present (*red arrowheads*). Note that cells not expressing the C terminus show green signal (*green arrow*), as subunit association is not disrupted. *B*, co-immunoprecipitation experiment showing TRPV1-HA interaction with TRPV1-YFP upon treatment with either DMSO (*Vehicle*), TRPV1 peptide (734–752), or scrambled peptide results. 200 μM palmitoylated peptide was incubated with intact cells for 1 h before lysis and immunoprecipitation with rat HA antibody. A western blot probed with anti-GFP of cell lysate (*Input*) and HA precipitates (*IP*; *bottom*) shows less association of TRPV1 subunits in the presence of TRPV1 peptide. A representative immunoblot (*IB*) of two independent experiments is shown. *C*, average calcium traces from cells expressing TRPV1 and TRPM8 and treated with 10 μM TRPV1 or scrambled peptides. The *black trace* represents the mean, and the *gray trace* represents the S.E. Response to capsaicin (*Cap.*) treatment relative to menthol-evoked response is attenuated in the TRPV1 peptide condition (*left*, $n = 56$) compared with the scrambled peptide condition (*right*, $n = 77$). *D*, average calcium traces in response to menthol (30 μM) from cells expressing TRPM8 and treated with 10 μM TRPV1 ($n = 89$) or scrambled peptides ($n = 51$). The *black trace* represents the mean, and the *gray trace* represents the S.E. *E*, concentration-response curve of TRPV1 peptide on capsaicin-evoked current. The I_{max} (elicited by a voltage step to +100 mV from a holding potential of 0 mV) was determined upon exposure to a saturating concentration of capsaicin (10 μM) in the absence of peptides ($n = 9$). Capsaicin-evoked current inhibition was measured after preincubation with 0.01, 0.1, 1, 5, 10, and 50 μM peptide ($n = 5$ per point). No statistically significant reduction was observed when cells were preincubated with the scrambled peptide at these concentrations. The capsaicin-evoked current inhibition was fitted with a Boltzmann equation.

TRPV1 Peptide 734–752 Interferes with Subunit Association—We next assessed whether the 734–751 peptide could reduce or abolish subunit association with an eye to its possible therapeutic use. Before tackling this with synthetic peptides, we first performed a proof-of-principle experiment to determine whether a membrane-tethered TRPV1 C terminus could reduce subunit interaction. We co-expressed CD4-Ct with VN-TRPV1 and VC-TRPV1 and used confocal imaging to determine if the BiFC signal would be lost when CD4-Ct is present, using a CD4-tagged N-terminal TRPV1 fragment (CD4-Nt2) as control. Cells expressing the hemi-Venus TRPV1 constructs as well as CD4-Nt2 show both Venus signal and CD4 signal (Fig. 5*A*, *top panels*). In contrast, cells co-transfected with CD4-Ct and hemi-Venus constructs show CD4 signal only (Fig. 5*A*, *bottom panels*, *red arrowheads*). Interestingly, cells in this condition that do not express the CD4-Ct do show Venus signal (Fig. 5*A*, *bottom panels*, *green arrow*), indicating that the CD4-Ct can interrupt the association between VN-TRPV1 and VC-TRPV1. We confirmed these data using co-precipitation of HA-TRPV1 and TRPV1-YFP. When CD4-Ct is co-expressed, less TRPV1-YFP precipitates with HA-TRPV1 compared with when CD4-AA or YFP-Ct are co-expressed (data not shown). Thus, a membrane-tethered TRPV1 C terminus interferes with subunit binding.

To disrupt channel assembly with our minimal motif, we used a peptide mimicking the TRPV1 residues 734–752 for *in vitro* and *in vivo* evaluation. Because the membrane-tethered CD4-Ct successfully disrupted TRPV1 subunit interaction, we chose an N-terminally palmitoylated synthetic peptide capable of associating with surface-expressed TRPV1 channels.

To test our peptide *in vitro*, we incubated cells expressing HA-TRPV1 and TRPV1-YFP with a saturating concentration (200 μM) of TRPV1 peptide, scrambled peptide, or vehicle only, then precipitated cell lysates using HA antibody. Immunoblotting for TRPV1-YFP indicates that TRPV1 peptide (residues 734–752) did indeed reduce co-immunoprecipitation of HA-TRPV1 with TRPV1-YFP (Fig. 5*B*).

We also tested the ability of the peptide to reduce TRPV1 function by measuring calcium influx in TRPV1 and TRPM8 co-transfected cells challenged with capsaicin and menthol as control. Cells incubated with TRPV1 peptide showed a markedly reduced capsaicin-evoked response despite having a pronounced response to menthol. Cells incubated with scrambled peptide, however, showed a robust response to capsaicin (Fig. 5*C*). Neither the TRPV1 nor scrambled peptides affected the menthol response in cells not exposed to capsaicin (Fig. 5*D*). Finally, the peptide-induced inhibition of capsaicin-evoked current was dose-dependent (Fig. 5*E*) with an IC_{50} of 4.52 μM as determined from the dose-response curve. These results strongly suggest that the TRPV1 synthetic peptide can prevent subunit association and thus TRPV1 function.

TRPV1 Peptide Attenuates Hyperalgesia in a Murine Model of Osteoarthritis and Carrageenan-induced Paw Edema—Having validated the efficacy of the palmitoylated TRPV1 peptide *in vitro*, we aimed to target channel function in an *in vivo* pain model that implicates TRPV1. Blockade of TRPV1 has been reported to be beneficial in several models of osteoarthritic pain (20). We used the MIA model of osteoarthritis in mice that presents ongoing mechanical hypersensitivity to evaluate the analgesic action of our peptide (21). Fifteen days after intra-articular injection of MIA, mice showed hallmarks of osteoarthritis in one knee; particularly, as previously reported, a decrease in mechanical pain threshold in response to Von Frey filaments applied to the ipsilateral (MIA-treated) but not the contralateral hind limb (saline). Mice received a hind paw injection of either TRPV1 peptide or scrambled peptide and were tested for mechanical hypersensitivity in both ipsilateral and contralateral hind limbs over 2 h. We observed a dose-dependent increase in the mechanical threshold in the ipsilateral side after TRPV1 peptide administration but not scrambled peptide (Fig. 6*A*, *left panel*). This reduction in mechanical sensitivity that reflects the anti-hyperalgesic action of the peptide was transient but significant at peptide concentrations $>$2.5 μM (Fig. 6*A*, *right panel*).

To test the central analgesic efficacy of the peptide, the mechanical sensitivity threshold was assessed on ipsilateral and contralateral sides after intrathecal administration of the peptide. Interestingly, we observed a similar reduction in mechanical hypersensitivity, revealed by an increase in mechanical threshold, for a 60-min period after injection of TRPV1 peptide, with a peak analgesic effect at 30 min. In contrast, injecting the scrambled peptide did not affect MIA-induced hypersensitivity (Fig. 6*B*).

As the TRPV1 channel has been noted to be a key contributor to thermal hyperalgesia in inflammation, we examined the efficacy of the peptide using Hargreaves' test of paw withdrawal after administration of 2% carrageenan. As shown in Fig. 6*C*, the TRPV1 peptide increases the latency of paw withdrawal at 30 and 60 min after initiation of the inflammatory insult, indicating a reduction in thermal hyperalgesia at these time points. Altogether, *in vivo* data using the membrane-tethered TRPV1 peptide support an anti-hyperalgesic action of TRPV1 disrupting moieties able to prevent interaction of channel subunits.

DISCUSSION

We have for the first time identified a minimal motif of 17 amino acids KDDYRWCFRVDEVNWTTW (residues 734–751) that mediates TRPV1 subunit association through direct interaction with their C-terminal domains. Removing this motif rendered the channel subunits unable to associate and hence abolished channel function. The more distal 752–772 region (previously identified as a tetrameric assembly domain (TAD)) also associated with the TRPV1 C terminus, corroborating the work of Zhang *et al.* (11). However, deleting these residues did not substantially reduce channel oligomerization and did not affect channel function, suggesting that either the TAD does not mediate subunit association but is involved in intramolecular interaction within the C terminus of a single TRPV1subunit or, alternatively, that the TAD may contribute to channel assembly but is not an essential element. Lending weight to the latter suggestion, the recently published structure of the assembled TRPV1 channel used a minimal functional rat TRPV1 lacking amino acids 764–838. Thus, removing a good portion of the TAD domain from purified TRPV1 channels did not prevent the formation of structurally stable tetramers (9).

In contrast, our data show that removing the more proximal residues 716–733 ablated both subunit association and channel function despite the fact that this region did not interact with the C terminus. There are several possible explanations for this finding. One possibility would be that removal of the 716–733 or 734–751 motif eliminates the capsaicin binding site on the channel; however, a substantial body of work has implicated the S2-S3 linker, including Tyr-511 and Ser-512, and the S4 domain, including Met-547 and Thr-550, in vanilloid binding (4, 22–26). A second explanation could be that the 716–733 region interacts with another part of the channel. Indeed, the TRPV1 cryo-EM structure has shown that a short unidentified stretch of the C terminus forms a β sheet with parts of the N terminus, which interacts directly with loops in the N-terminal ankyrin repeat domain of an adjacent subunit (9); residues 716–733 may contribute to channel oligomerization in this way. A third possibility is simply that removing this stretch of residues shifted the adjacent assembly motif (residues 734–751) out of reach of its interacting target, rendering the subunit unable to associate despite having the association residues intact. The channel structure, although illuminating, does not reveal which of these scenarios may be occurring. Further experiments are required to determine the significance of these residues.

The function of the 734–751 motif may not be restricted to mediating TRPV1 subunit assembly. Zhang *et al.* (27) identified the residues KDDYRWCFRVDEVN, corresponding to amino acids 736–749 of human TRPV1, to be the binding site for AKAP79. A kinase anchoring proteins (AKAPs) define a group of scaffolding proteins involved in optimizing TRPV1 channel phosphorylation. Interaction between AKAP79 and TRPV1 has

been found to be a prerequisite for PKA- and PKC-dependent sensitization of TRPV1 (27–29). Removing the 736–749 of TRPV1 region abolished its binding to AKAP, and a peptide mimicking these residues interfered with TRPV1-AKAP association. Interestingly, recent work from the same group used a cell-penetrating TAT-conjugated form of this peptide to prevent TRPV1 sensitization induced by inflammatory mediators *in vitro* and to alleviate inflammatory hyperalgesia *in vivo* (30). Because the residues of TRPV1 we identified as the subunit assembly domain overlap with this AKAP binding motif, we

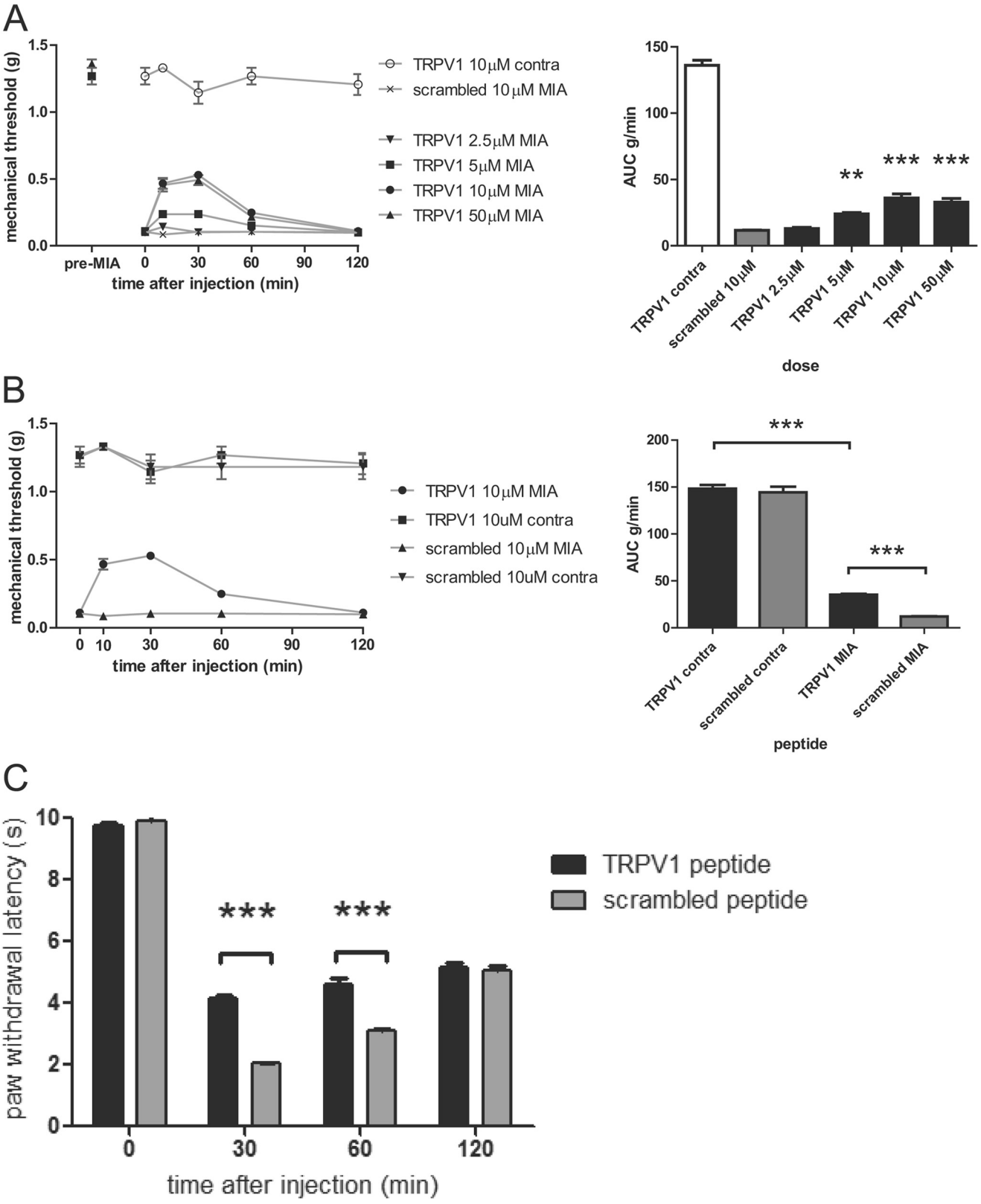

cannot rule out that our peptide prevents AKAP binding to the channel *in vivo*. However, we confirmed that deleting these residues from the channel abrogates channel function, and infusion of our peptide disrupts subunit-subunit interaction *in vitro*. Therefore, it seems unlikely that the AKAP binding domain overlaps with the TRPV1 assembly domain, as this would make subunit association and AKAP binding mutually exclusive. Instead, we postulate that TRPV1 subunit assembly, at least dimerization, is required for AKAP association and phosphorylation-dependent sensitization of the channel *in vivo*. TRPV1 has indeed been shown to be in dimeric form at the plasma membrane and able to tetramerize upon activation with the TRPV1 agonist resiniferatoxin (31). Interestingly, this study reported a dynamic interaction between TRPV1 homomers and polymerized microtubules that appears crucial for regulating TRPV1 functionality. Perhaps the TRPV1 peptide can also alter TRPV1-microtubule interaction by disrupting associated TRPV1 subunits. Hence, future work is warranted to understand the mechanisms whereby cytoskeletal proteins or signaling molecules interact with homomeric forms of TRPV1 to regulate channel function. Our data nevertheless are in complete agreement with previous work that showed this short region of TRPV1, which governs subunit association, to be critical for channel function.

Over the past decade TRPV1 channel has been recognized as a critical sensor for physical and bioactive molecules that exacerbate pain sensation during peripheral sensitization associated with inflammatory conditions (6). Although TRPV1 antagonists may represent a novel pharmacological cornerstone in pain management, their clinical use has been limited by hyperthermic side effects (32). Current investigations are centered on separating the analgesic potency of TRPV1 blockers from their hyperthermic action. Our results validate the anti-hyperalgesic properties of TRPV1 peptides that disrupt channel subunit assembly. Indeed, a palmitoylated peptide, which mimics the TRPV1 subunit interaction domain, was able to attenuate pain in mouse models of both osteoarthritis and thermal hyperalgesia. Thus, targeting TRPV1 subunit assembly to diminish overall TRPV1 function, rather than blocking channels *in situ*, may present an untapped vein of pharmacological therapy in pain management.

TRPV1 is an essential component of the cellular signaling mechanisms through which tissue damage or infection produces thermal hyperalgesia and pain hypersensitivity (4, 7, 33). Here, using the carrageenan model of inflammatory pain we observed an increase in the threshold of thermal pain for 1 h after injection of the peptide, highlighting the anti-hyperalgesic effect of disrupting TRPV1 subunit association *in vivo*. Numerous studies have described the contribution of TRPV1 to the establishment of osteoarthritis-induced mechanical hypersensitivity in humans and in animal models (34–38), suggesting that inhibition of TRPV1 *in vivo* is a viable target for the relief of osteoarthritis pain. Accordingly, administration of the TRPV1 antagonist A-995662 was shown to attenuate mechanical pain in osteoarthritic rats through its ability to inhibit glutamate and CGRP (calcitonin gene-related peptide) release from primary afferent terminals in the dorsal horn of the spinal cord (20). The authors found that 100 μmol/kg could reverse 80% of osteoarthritis mechanical pain. In a different study, Chu *et al.* (39) described the analgesic effect of A-889425 on MIA-induced pain and its inhibition of spinal responses to mechanical stimulation. At the highest dose tested (300 μmol/kg, orally), A-889425 fully reversed the osteoarthritis-induced grip force impairment. Our results show that 50 μM TRPV1 peptide blocks nearly 50% of osteoarthritis pain, indicating that the degree of analgesia observed with our peptide is still inferior to a TRPV1 antagonist. We think that this could be due to a limited diffusion of the peptide locally and a rapid degradation of the peptide once injected. In this regard, the majority of the work on TRPV1 in pain signaling has focused on targeting the channel in nociceptor endings at the periphery. However, recent studies have highlighted its functional influence at the spinal level. TRPV1 was shown to be functionally expressed in GABAergic spinal interneurons where its activation leads to mechanical allodynia (40). In addition, TRPV1 likely contributes to the descending facilitation of osteoarthritis pain at the spinal level (41). Although we can not ascertain whether central or peripheral TRPV1 is the major contributor of mechanical hypersensitivity in our model, our findings with the intrathecal administration of the peptide support that spinal inhibition of TRPV1 channel enables pain relief in MIA-induced osteoarthritis. Of note, others have shown that antagonists of TRPV1 block MIA-induced thermal hyperalgesia but not weight asymmetry or ongoing pain (37). Finally, stimulation of capsaicin-sensitive sensory neurons appeared to reduce both pain and bone lesions in the MIA model (42). Overall, our results support the view that blocking TRPV1 function promotes analgesia in osteoarthritis and present an alternative therapeutic strategy centered on tailoring channel function by preventing subunit association rather than blocking allosteric activation.

The utilization of a membrane-tethered peptide in our *in vivo* experiments is supported by recent FRET analysis that determined the proximity of TRPV1 terminal domains to the plasma membrane (43). In this study the authors were able to show that the C terminus was closer to the plasma membrane than the N terminus, which suggests that, once incorporated

FIGURE 6. **TRPV1 peptide ameliorates both mechanical and thermal hyperalgesia.** *A*, intrathecal injection of TRPV1 peptide reduces mechanical pain threshold in MIA-induced osteoarthritic mice. Mice injected with MIA into the knee joint were treated with either TRPV1 or scrambled peptide. *Left panel*, dose-response curves for TRPV1 peptide showing mechanical withdrawal threshold in the ipsilateral MIA and contralateral side after TRPV1 or scrambled peptide injection. *Right panel*, *bar graph* representing the area under the curve (*AUC*) of the mechanical threshold data presented in the *left panel*. $n = 6–8$ per group. **, $p < 0.05$; ***, $p < 0.01$ compared with the MIA group injected with scrambled peptide, one-way ANOVA. *B*, intraplantar injection of TRPV1 peptide into the ipsilateral hind paw reduces mechanical pain threshold in MIA-induced osteoarthritic mice. *Left panel*, TRPV1 peptide increases mechanical withdrawal threshold as compared with scrambled peptide. *Right panel*, *bar graph* representing the area under the curve of the mechanical threshold data presented in the *left panel*. $n = 6–8$ per group. ***, $p < 0.01$ compared with the MIA group injected with scrambled or TRPV1 peptide, one-way ANOVA. *C*, TRPV1 peptide attenuates inflammatory thermal hyperalgesia. Mice that received intraplantar injections of 2% carrageenan along with 10 μM concentrations of either TRPV1 or scrambled peptide were tested at different time points for latency of paw withdrawal in response to radiant heat. $n = 6–7$ per group. ***. $p < 0.01$ using two-way ANOVA.

into the membrane, our palmitoylated TRPV1 peptide would likely have access to the C terminus to disrupt subunit assembly. Accordingly, other studies have reported a therapeutic benefit from administration of a membrane-tethered TRPV1 fragment (44). Collectively, our findings suggest that the TRPV1 assembly domain identified in the C-terminal region of the channel could represent a viable target for the development of novel types of TRPV1 blockers, thus paving the way for developing alternative avenues in modern pain therapy.

Acknowledgments—We thank Dr. Gerald Zamponi for providing the BiFC leucine zipper vectors. We thank Dr. Jason McDougall for helping to establish the MIA model. We thank Arun Teja Veeramalla for technical assistance.

REFERENCES

1. Caterina, M. J., Schumacher, M. A., Tominaga, M., Rosen, T. A., Levine, J. D., and Julius, D. (1997) The capsaicin receptor: a heat-activated ion channel in the pain pathway. *Nature* **389,** 816–824
2. Szallasi, A., and Blumberg, P. M. (1993) [^{3}H]Resiniferatoxin binding by the vanilloid receptor: species-related differences, effects of temperature and sulfhydryl reagents. *Naunyn Schmiedebergs Arch. Pharmacol.* **347,** 84–91
3. Bohlen, C. J., Priel, A., Zhou, S., King, D., Siemens, J., and Julius, D. (2010) A bivalent tarantula toxin activates the capsaicin receptor, TRPV1, by targeting the outer pore domain. *Cell* **141,** 834–845
4. Julius, D. (2013) TRP channels and pain. *Annu. Rev. Cell Dev. Biol.* **29,** 355–384
5. Zygmunt, P. M., Petersson, J., Andersson, D. A., Chuang, H., Sørgård, M., Di Marzo, V., Julius, D., and Högestätt, E. D. (1999) Vanilloid receptors on sensory nerves mediate the vasodilator action of anandamide. *Nature* **400,** 452–457
6. Bourinet, E., Altier, C., Hildebrand, M. E., Trang, T., Salter, M. W., and Zamponi, G. W. (2014) Calcium-permeable ion channels in pain signaling. *Physiol. Rev.* **94,** 81–140
7. Caterina, M. J., Leffler, A., Malmberg, A. B., Martin, W. J., Trafton, J., Petersen-Zeitz, K. R., Koltzenburg, M., Basbaum, A. I., and Julius, D. (2000) Impaired nociception and pain sensation in mice lacking the capsaicin receptor. *Science* **288,** 306–313
8. Karai, L., Brown, D. C., Mannes, A. J., Connelly, S. T., Brown, J., Gandal, M., Wellisch, O. M., Neubert, J. K., Olah, Z., and Iadarola, M. J. (2004) Deletion of vanilloid receptor 1-expressing primary afferent neurons for pain control. *J. Clin. Invest.* **113,** 1344–1352
9. Liao, M., Cao, E., Julius, D., and Cheng, Y. (2013) Structure of the TRPV1 ion channel determined by electron cryo-microscopy. *Nature* **504,** 107–112
10. García-Sanz, N., Fernández-Carvajal, A., Morenilla-Palao, C., Planells-Cases, R., Fajardo-Sánchez, E., Fernández-Ballester, G., and Ferrer-Montiel, A. (2004) Identification of a tetramerization domain in the C terminus of the vanilloid receptor. *J. Neurosci.* **24,** 5307–5314
11. Zhang, F., Liu, S., Yang, F., Zheng, J., and Wang, K. (2011) Identification of a tetrameric assembly domain in the C terminus of heat-activated TRPV1 channels. *J. Biol. Chem.* **286,** 15308–15316
12. Covic, L., Gresser, A. L., Talavera, J., Swift, S., and Kuliopulos, A. (2002) Activation and inhibition of G protein-coupled receptors by cell-penetrating membrane-tethered peptides. *Proc. Natl. Acad. Sci. U.S.A.* **99,** 643–648
13. Robitaille, M., Héroux, I., Baragli, A., and Hébert, T. E. (2009) Novel tools for use in bioluminescence resonance energy transfer (BRET) assays. *Methods Mol. Biol.* **574,** 215–234
14. Héroux, M., Hogue, M., Lemieux, S., and Bouvier, M. (2007) Functional calcitonin gene-related peptide receptors are formed by the asymmetric assembly of a calcitonin receptor-like receptor homo-oligomer and a monomer of receptor activity-modifying protein-1. *J. Biol. Chem.* **282,** 31610–31620
15. Liu, H., and Naismith, J. H. (2008) An efficient one-step site-directed deletion, insertion, single and multiple-site plasmid mutagenesis protocol. *BMC Biotechnol.* **8,** 91
16. Altier, C., Garcia-Caballero, A., Simms, B., You, H., Chen, L., Walcher, J., Tedford, H. W., Hermosilla, T., and Zamponi, G. W. (2011) The Cavβ subunit prevents RFP2-mediated ubiquitination and proteasomal degradation of L-type channels. *Nat. Neurosci.* **14,** 173–180
17. Dixon, W. J. (1980) Efficient analysis of experimental observations. *Annu. Rev. Pharmacol. Toxicol.* **20,** 441–462
18. Chaplan, S. R., Bach, F. W., Pogrel, J. W., Chung, J. M., and Yaksh, T. L. (1994) Quantitative assessment of tactile allodynia in the rat paw. *J. Neurosci. Methods* **53,** 55–63
19. Wang, S., and Chuang, H. H. (2011) C-terminal dimerization activates the nociceptive transduction channel transient receptor potential vanilloid 1. *J. Biol. Chem.* **286,** 40601–40607
20. Puttfarcken, P. S., Han, P., Joshi, S. K., Neelands, T. R., Gauvin, D. M., Baker, S. J., Lewis, L. G., Bianchi, B. R., Mikusa, J. P., Koenig, J. R., Perner, R. J., Kort, M. E., Honore, P., Faltynek, C. R., Kym, P. R., and Reilly, R. M. (2010) A-995662 ((*R*)-8-(4-methyl-5-(4-(trifluoromethyl)phenyl)oxazol-2-ylamino)-1,2,3,4-tetrahydronaphthalen-2-ol), a novel, selective TRPV1 receptor antagonist, reduces spinal release of glutamate and CGRP in a rat knee joint pain model. *Pain* **150,** 319–326
21. Harvey, V. L., and Dickenson, A. H. (2009) Behavioural and electrophysiological characterisation of experimentally induced osteoarthritis and neuropathy in C57Bl/6 mice. *Mol. Pain* **5,** 18
22. Gavva, N. R., Klionsky, L., Qu, Y., Shi, L., Tamir, R., Edenson, S., Zhang, T. J., Viswanadhan, V. N., Toth, A., Pearce, L. V., Vanderah, T. W., Porreca, F., Blumberg, P. M., Lile, J., Sun, Y., Wild, K., Louis, J. C., and Treanor, J. J. (2004) Molecular determinants of vanilloid sensitivity in TRPV1. *J. Biol. Chem.* **279,** 20283–20295
23. Jung, J., Hwang, S. W., Kwak, J., Lee, S. Y., Kang, C. J., Kim, W. B., Kim, D., and Oh, U. (1999) Capsaicin binds to the intracellular domain of the capsaicin-activated ion channel. *J. Neurosci.* **19,** 529–538
24. Jordt, S. E., and Julius, D. (2002) Molecular basis for species-specific sensitivity to "hot" chili peppers. *Cell* **108,** 421–430
25. Phillips, E., Reeve, A., Bevan, S., and McIntyre, P. (2004) Identification of species-specific determinants of the action of the antagonist capsazepine and the agonist PPAHV on TRPV1. *J. Biol. Chem.* **279,** 17165–17172
26. Cao, E., Liao, M., Cheng, Y., and Julius, D. (2013) TRPV1 structures in distinct conformations reveal activation mechanisms. *Nature* **504,** 113–118
27. Zhang, X., Li, L., and McNaughton, P. A. (2008) Proinflammatory mediators modulate the heat-activated ion channel TRPV1 via the scaffolding protein AKAP79/150. *Neuron* **59,** 450–461
28. Schnizler, K., Shutov, L. P., Van Kanegan, M. J., Merrill, M. A., Nichols, B., McKnight, G. S., Strack, S., Hell, J. W., and Usachev, Y. M. (2008) Protein kinase A anchoring via AKAP150 is essential for TRPV1 modulation by forskolin and prostaglandin E2 in mouse sensory neurons. *J. Neurosci.* **28,** 4904–4917
29. Jeske, N. A., Patwardhan, A. M., Ruparel, N. B., Akopian, A. N., Shapiro, M. S., and Henry, M. A. (2009) A-kinase anchoring protein 150 controls protein kinase C-mediated phosphorylation and sensitization of TRPV1. *Pain* **146,** 301–307
30. Fischer, M. J., Btesh, J., and McNaughton, P. A. (2013) Disrupting sensitization of transient receptor potential vanilloid subtype 1 inhibits inflammatory hyperalgesia. *J. Neurosci.* **33,** 7407–7414
31. Storti, B., Bizzarri, R., Cardarelli, F., and Beltram, F. (2012) Intact microtubules preserve transient receptor potential vanilloid 1 (TRPV1) functionality through receptor binding. *J. Biol. Chem.* **287,** 7803–7811
32. Moran, M. M., McAlexander, M. A., Bíró, T., and Szallasi, A. (2011) Transient receptor potential channels as therapeutic targets. *Nat. Rev. Drug Discov.* **10,** 601–620
33. Basbaum, A. I., Bautista, D. M., Scherrer, G., and Julius, D. (2009) Cellular and molecular mechanisms of pain. *Cell* **139,** 267–284
34. Vonsy, J. L., Ghandehari, J., and Dickenson, A. H. (2009) Differential analgesic effects of morphine and gabapentin on behavioural measures of pain and disability in a model of osteoarthritis pain in rats. *Eur. J. Pain* **13,** 786–793

35. Ogbonna, A. C., Clark, A. K., Gentry, C., Hobbs, C., and Malcangio, M. (2013) Pain-like behaviour and spinal changes in the monosodium iodoacetate model of osteoarthritis in C57Bl/6 mice. *Eur. J. Pain* **17,** 514–526
36. Kelly, S., Chapman, R. J., Woodhams, S., Sagar, D. R., Turner, J., Burston, J. J., Bullock, C., Paton, K., Huang, J., Wong, A., McWilliams, D. F., Okine, B. N., Barrett, D. A., Hathway, G. J., Walsh, D. A., and Chapman, V. (2013) Increased function of pronociceptive TRPV1 at the level of the joint in a rat model of osteoarthritis pain. *Ann. Rheum Dis.* 10.1136/annrheumdis-2013–203413
37. Okun, A., Liu, P., Davis, P., Ren, J., Remeniuk, B., Brion, T., Ossipov, M. H., Xie, J., Dussor, G. O., King, T., and Porreca, F. (2012) Afferent drive elicits ongoing pain in a model of advanced osteoarthritis. *Pain* **153,** 924–933
38. Honore, P., Chandran, P., Hernandez, G., Gauvin, D. M., Mikusa, J. P., Zhong, C., Joshi, S. K., Ghilardi, J. R., Sevcik, M. A., Fryer, R. M., Segreti, J. A., Banfor, P. N., Marsh, K., Neelands, T., Bayburt, E., Daanen, J. F., Gomtsyan, A., Lee, C. H., Kort, M. E., Reilly, R. M., Surowy, C. S., Kym, P. R., Mantyh, P. W., Sullivan, J. P., Jarvis, M. F., and Faltynek, C. R. (2009) Repeated dosing of ABT-102, a potent and selective TRPV1 antagonist, enhances TRPV1-mediated analgesic activity in rodents, but attenuates antagonist-induced hyperthermia. *Pain* **142,** 27–35
39. Chu, K. L., Chandran, P., Joshi, S. K., Jarvis, M. F., Kym, P. R., and McGaraughty, S. (2011) TRPV1-related modulation of spinal neuronal activity and behavior in a rat model of osteoarthritic pain. *Brain Res.* **1369,** 158–166
40. Kim, Y. H., Back, S. K., Davies, A. J., Jeong, H., Jo, H. J., Chung, G., Na, H. S., Bae, Y. C., Kim, S. J., Kim, J. S., Jung, S. J., and Oh, S. B. (2012) TRPV1 in GABAergic interneurons mediates neuropathic mechanical allodynia and disinhibition of the nociceptive circuitry in the spinal cord. *Neuron* **74,** 640–647
41. Zhang, R. X., Ren, K., and Dubner, R. (2013) Osteoarthritis pain mechanisms: basic studies in animal models. *Osteoarthritis Cartilage* **21,** 1308–1315
42. Kalff, K. M., El Mouedden, M., van Egmond, J., Veening, J., Joosten, L., Scheffer, G. J., Meert, T., and Vissers, K. (2010) Pre-treatment with capsaicin in a rat osteoarthritis model reduces the symptoms of pain and bone damage induced by monosodium iodoacetate. *Eur. J. Pharmacol.* **641,** 108–113
43. De-la-Rosa, V., Rangel-Yescas, G. E., Ladrón-de-Guevara, E., Rosenbaum, T., and Islas, L. D. (2013) Coarse architecture of the transient receptor potential vanilloid 1 (TRPV1) ion channel determined by fluorescence resonance energy transfer. *J. Biol. Chem.* **288,** 29506–29517
44. Valente, P., Fernández-Carvajal, A., Camprubí-Robles, M., Gomis, A., Quirce, S., Viana, F., Fernández-Ballester, G., González-Ros, J. M., Belmonte, C., Planells-Cases, R., and Ferrer-Montiel, A. (2011) Membrane-tethered peptides patterned after the TRP domain (TRPducins) selectively inhibit TRPV1 channel activity. *FASEB J.* **25,** 1628–1640